Unraveling Hydrogen Atom Transfer Mechanisms with Voltammetry: Oxidative Formation and Reactivity of Cobalt Hydride

Dylan G. Boucher†, Andrew D. Pendergast†, Xiangyu Wu‡, Zachary A. Nguyen†, Song Lin‡, Henry S. White†, and Shelley D. Minteer†*

*Denotes corresponding author: minteer@chem.utah.edu

†Department of Chemistry, University of Utah, Salt Lake City, UT

‡Department of Chemistry, Cornell University, Ithaca, NY

ABSTRACT

The utility of transition metal hydride catalyzed hydrogen atom transfer (MHAT) has been widely demonstrated in organic transformations such as alkene isomerization and hydrofunctionalization reactions. However, the highly reactive nature of the hydride and radical intermediates has hindered mechanistic insight into this pivotal reaction. Recent advances in electrochemical MHAT have opened the possibility for new analytical approaches for mechanistic diagnosis. Here, we report a voltammetric interrogation of Co-based MHAT reactivity, describing in detail the oxidative formation and reactivity of the key Co-H intermediate and its reaction with aryl alkenes. Insights from cyclic voltammetry and finite element simulations help elucidate the rate-limiting step as metal hydride formation, which we show to be widely tunable based on ligand design. Voltammetry is also suggestive of the formation of Co-alkyl intermediates and a dynamic equilibrium with the reactive neutral radical. These mechanistic studies provide information for the design of future hydrofunctionalization reactions, such as catalyst and silane choice, the relative stability of metal-alkyl species, and how hydrofunctionalization reactions utilize Co-alkyl intermediates. In summary, these studies establish an important template for studying MHAT reactions from the perspective of electrochemical kinetic frameworks.

1. Introduction

In the past decade, metal hydride mediated hydrogen atom transfer (MHAT) has emerged as a dominant mode of achieving hydrofunctionalization reactions of alkenes.[1] Utilizing the homolytic reactivity of a transition metal hydride catalyst, this reaction mode features the concerted movement of a proton and electron (thus stoichiometrically an H atom equivalent) from the catalyst to the substrate to generate a reactive radical intermediate that can be captured in a wide array of alkene hydrofunctionalization reactions (**Scheme 1a**), such as hydroalkoxylation,[2] hydrocyanation,[3] and hydrocarbonation,[4, 5] alkene isomerization reactions,[6] and many others.[7] MHAT reactivity with alkenes has also found utility as a method of radical initiated polymerization.[8] The unique homolytic reactivity MHAT imparts to alkenes, as well as the versatility in its application, has made this an indispensable tool in the modern synthetic chemist's tool kit.

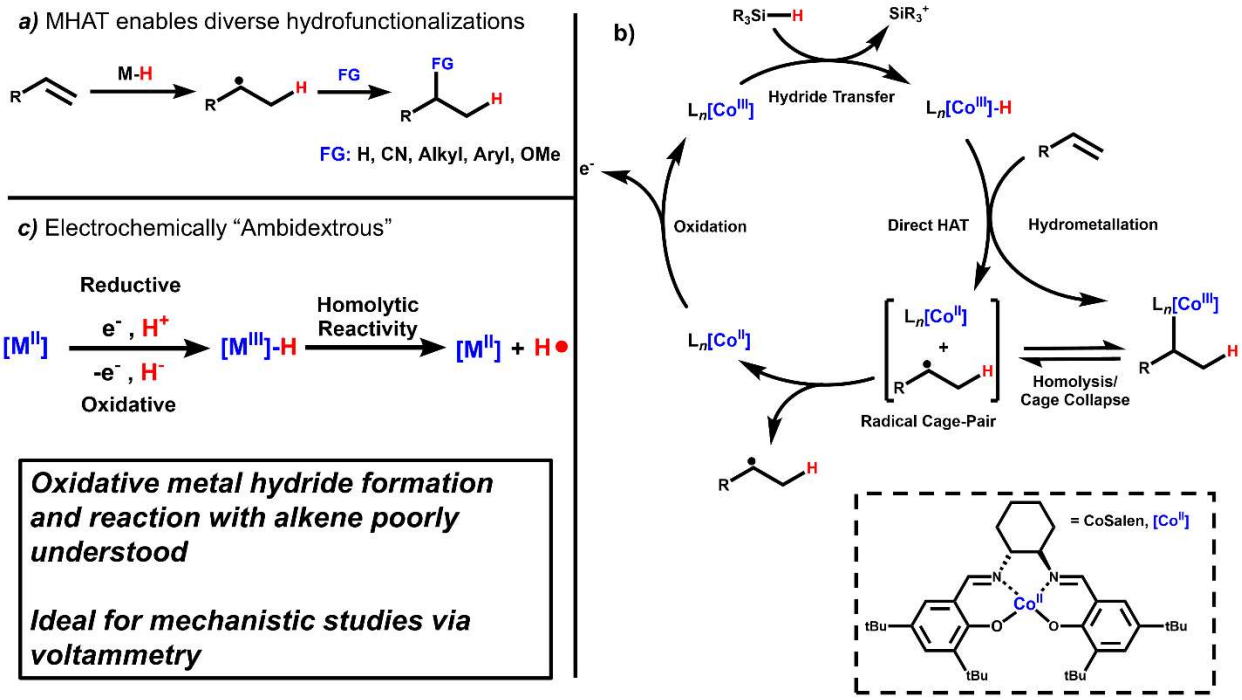

Scheme 1. Overview of a) the homolytic reactivity of metal hydride species, b) the modern understanding of the mechanism, and c) and their oxidative and reductive formation.

Despite the synthetic utility of MHAT reactions, direct mechanistic characterization of the transient hydride and radical intermediates has proved challenging. Much of the difficulty in mechanistic analysis stems from the weak field (WF) nature of the ligands used to achieve MHAT.[7, 9] While strong field (SF) ligand metal hydride complexes are relatively stable and isolable,[10] these ligands tend to promote polar reactivity, such as hydrogen evolution,[10] hydride donation (i.e. hydrogenation),[11] or HAT to electron-deficient alkenes.[12] In contrast, the weak metal-hydride bond in weak field (WF) ligand metal hydride complexes readily dissociates homolytically to promote radical reactivity while also rendering such complexes short-lived and difficult to isolate or even observe experimentally.[7] The MHAT reaction itself is estimated to proceed extremely fast and irreversibly, and the speed of this step often prevents it from being measured directly.[13] In fact, computational studies have estimated the working concentration of metal hydride species during MHAT reactions to be as low as 10^{-16} M (in the presence of alkene substrate).[13] As a result, not much is known about the formation or reaction of this intermediate outside of what qualitative studies and historical evidence of SF metal hydrides can explain; however, the exact design principles for the homolytic reactivity of these catalytic intermediates are likely to be quite different.

Furthermore, the exact nature of the H atom transfer step is debated. The original synthetic work pioneered by Mukaiyama[14] was postulated to proceed via a hydrometallation pathway and the formation of an organometallic intermediate.[15] In contrast, a more modern understanding of MHAT reactivity is most consistent with a direct H atom transfer step to form the neutral radical organic intermediate, which can then freely react with radical electrophiles (**Scheme 1b**).[6] These divergent mechanisms are further complicated by the fact that the products of each, the organometallic intermediate and the neutral radical organic species, likely exist in a dynamic equilibrium between the two via cage-collapse and organometallic homolysis.[6, 16] Despite observed reactivity supporting the neutral radical, mechanistic studies of dual catalytic systems showed the rate-determining step to involve

transmetallation from the metal-alkyl intermediate.[17] Such results indicate that MHAT reactions likely utilize both neutral radical and metal-alkyl intermediates to achieve their diverse reactivity. Thus, the exact balance of this step depends on the nature of the alkene substrate, the reactivity of the metal hydride, *as well as* the stability of the metal-alkyl bound intermediate. Direct investigation of these intermediates is not often possible, leading researchers to depend on product analysis for their mechanistic insights, which has limited utility in the rational design of catalysts and predicting new modes of reactivity. Methods of direct mechanistic investigation are greatly needed.

The recent advent of electrochemical MHAT (e-MHAT) reactions has opened the door to direct mechanistic diagnosis. In traditional MHAT organometallic reactions, the metal-hydride is generated by hydride transfer from a hydride donor (such as phenylsilane); thus, the catalytic cycle requires an external oxidant to assist in the conversion of a hydride (H^-) to an H atom (**Scheme 1c**). To this end, electrochemical generation of the metal hydride has offered an alternative to access MHAT reactivity without needing to consider the compatibility of the catalyst, oxidant, and hydride source while also providing direct information about the charge consumed by the catalyst. Lin and coworkers demonstrated the power of this technique with an enantioselective hydrocyanation reaction of aryl-alkenes.[18] Zhu and coworkers have similarly utilized this oxidative MHAT pathway to achieve a wide-array of electrochemical hydroalkoxylation and hydroarylation products.[19] In addition, Baran and co-workers have illustrated the reductive generation of cobalt hydride species from protons to carry out MHAT reactions with alkenes.[20] Likewise, the Lin group has realized alkene hydroarylation and deuteration reactions via reductive e-MHAT.[21] The 'ambidextrous' generation of reactive metal hydrides via either oxidative or reductive modes enables e-MHAT reactions to be adapted to a wide range of solvents, electrophiles, and co-catalysts[22] that may be unstable when subject to opposite electrochemical polarities.

Electrochemical MHAT reactions are not only exciting from a synthetic point of view, but they also enable in-depth electroanalytical analysis of the reaction mechanism via direct access to the catalyst

concentration, redox state, and charge consumed during catalysis.[23] Cyclic voltammetry (CV) has been long established as a quantitative analytical technique for studying chemical thermodynamics, kinetics, and mechanisms.[24] It has been used for decades to study the reductive generation of metal hydride complexes from protons for hydrogen evolution reactions[25-27] and has recently been extended to *reductive* e-MHAT studies.[21] A similar approach has been utilized with great effect to study the mechanism of concerted proton electron transfer (CPET) mediation to ketones[28] and alkenes[29], a conceptually similar process to reductive e-MHAT. In contrast, the oxidative pathway, the oxidation of a hydride to hydrogen atom, has not been studied with these powerful electroanalytical techniques, and doing so could help provide important mechanistic insights into MHAT reactions, even beyond those carried out electrocatalytically.

Here, cyclic voltammetric studies of Co(Salen) provide a valuable mechanistic framework to understand these multi-step catalytic reactions, with insights into both electrochemical and traditional synthetic modes. Using a model homolytic model reaction, we establish rate constants for cobalt hydride formation and show that hydride transfer is the rate-determining step for MHAT reactions. Using a series of modified salen ligands, we show the rate of hydride transfer is tunable, suggesting further mechanistic control in future MHAT reactions. Finally, the Co-H reaction with aryl alkenes is also studied to observe and quantify the dynamic equilibrium between the Co-alkyl species and the neutral radical, with experimental evidence that MHAT progresses through the hydrometallation pathway. In summary, these mechanistic studies provide important information for the design of future hydrofunctionalization reactions such as catalyst and silane choice, the relative metal-alkyl intermediates, and how MHAT reactions utilize the bimodal reactivity of both Co-alkyl intermediates and neutral radical intermediates. Additionally, these studies establish an important template for studying complex HAT reaction mechanisms using electroanalytical techniques.

2. Results and Discussion

Probing mechanism of Co-H formation via cyclic voltammetry

In order to probe the formation and reactivity of Co-H, we utilized cyclic voltammetry to study Co(Salen) (specifically the cyclohexyl ligand, **Scheme 1b**) and its reaction with the common hydride donor phenylsilane. Co(Salen) exhibited reversible redox behavior both at -1.95 V vs $Fc^{+/o}$ (Co(I/II) couple) and -0.48 V vs $Fc^{+/o}$ (Co(II/III)), as shown in **Figure S1**. The redox peak of interest here is the oxidative Co(II/III) couple, which exhibited reversibility over a wide range of scan rates (**Figure S2**). The addition of the hydride donor species phenylsilane altered this reversible behavior results in the decrease of the return wave (Co(III) reduction) and an increase in the current of the forward wave (Co(II) oxidation). This behavior is consistent with electrocatalytic activity (**Figure 1a**).[27] At high silane concentrations, the peak shape is sigmoidal, indicative of the catalytic behavior of an electrocatalytic system under kinetic control.[24] Analysis of the normalized plateau current, i_{cat} (normalized to the peak current when no phenylsilane is present, i_p^0) with respect to the square root of the amount of phenylsilane added revealed two distinct regions at low and high concentrations of silane (**Figure 1b**). Namely, the normalized peak current varies linearly with respect to the concentration at low silane concentrations (**Figure 1b inset,** and **Figure S3**) and exhibits a linear dependence with respect to the square-root of concentration at high silane concentrations.

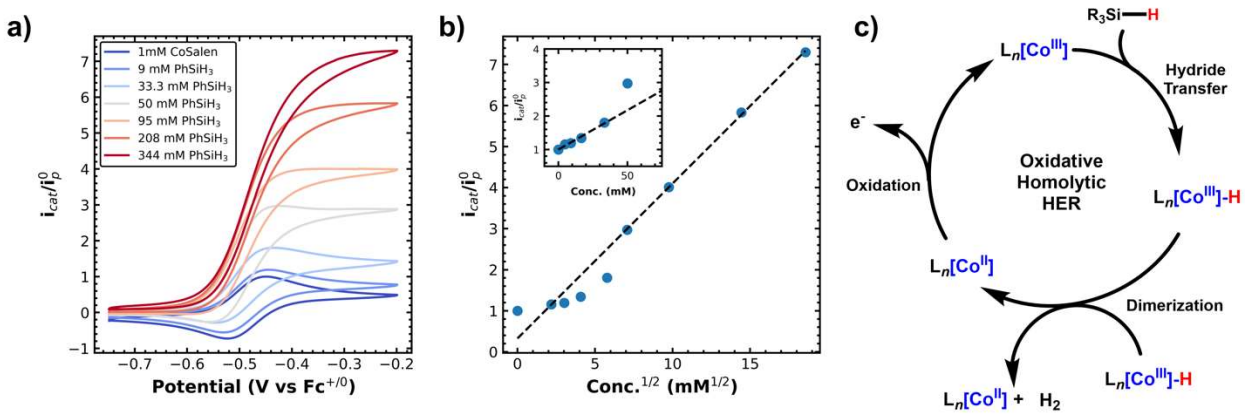

Figure 1. *a)* Cyclic voltammetry of Co(Salen) oxidation (Co(II)/Co(III) couple) with increasing amounts of hydride donor phenylsilane in a solution of 0.1 M $TBAPF_6$ in DMF with a glassy carbon working electrode at 10 mV/s. *b)* Peak current analysis revealed a linear trend with square root of concentration at high silane concentrations, indicating metal-hydride formation via hydride transfer as the rate-limiting step (inset shows low silane concentration). *c)* Proposed catalytic cycle for the oxidative formation of Co-H and subsequent dimerization (reaction of two Co-H to produce H_2).

To account for this voltammetric behavior we propose an oxidative homolytic hydrogen evolution catalytic cycle (**Figure 1c.**) This cycle consists of the initial oxidation of Co(Salen) from Co(II) to Co(III), which then abstracts a hydride from phenylsilane in a hydride transfer step resulting in Co(III)-H. Finally, this Co(III)-H species undergoes a dimerization step with another Co(III)-H species to yield two equivalents of Co(II)(Salen) and an equivalent of H_2. Though this reaction is not useful from a synthetic or energy storage perspective, it is a useful model reaction through which we can understand the kinetics and mechanism of Co(III)-H formation and study its reactivity. For example, in the framework developed by Savéant and Constentin, the dependence of the peak current on substrate concentration contains important mechanistic information.[30] The common EC' mechanism (one subsequent chemical step which returns the original catalyst state) exhibits a square root dependence of substrate concentration as demonstrated by equation 1:

$$i_{cat} = nFAC_{cat}(D_{cat}k_1C_A)^{1/2} \quad (1)$$

where i_{cat} is the catalytic plateau current, n is the number of electrons involved in the transfer, F is Faraday's constant, C_{cat} is the concentration of the catalyst, D_{cat} is the diffusion constant of the catalyst, k_1 is the rate constant of the chemical step, and C_A is the concentration of the substrate. It is important to note that this equation describes a first-order rate dependence on substrate concentration,[31] but the limiting current is proportional to the square-root based on diffusion of the catalyst. In **Figure 1b** at low silane concentrations, the peak current is linear with respect to the substrate concentration (see inset); however, at high concentrations, the peak current has a square root dependence on substrate concentration predicted by an EC' mechanism.

The transition from one dependence to another is indicative of a change in the rate-determining step (RDS) of our proposed mechanism. At low silane concentrations, the dependence suggests that dimerization is rate limiting, but at high silane concentrations, hydride transfer is the RDS. The shift in RDS indicates that the subsequent dimerization occurs quickly relative to hydride transfer step (and thus behaves like an EC' mechanism, and is first order with respect to the silane). The rate of dimerization at low silane concentrations is likely slow, not because the reaction itself is slow, but because the concentration of Co-H is low, thus inhibiting the rate of the bimolecular reaction. Further evidence of the EC' behavior at high silane concentrations can be seen in the peak current dependence on catalyst concentration: **Figure 2a** shows the CVs of varying Co(Salen) concentrations at 1000 eq of phenylsilane (0.33 M) and **Figure 2b** shows this dependence is linear with respect to the catalyst concentration (i.e. the reaction is first order in catalyst). The linear dependence of peak current on the catalyst concentration is predicted by equation 1 for an EC' like mechanism. In addition, the hydride transfer step and hydride formation are dependent on the identity of the hydride donor. Substitution of phenylsilane with triethylsilane, a weaker hydride donor, slows down catalysis significantly (**Figure S4**).

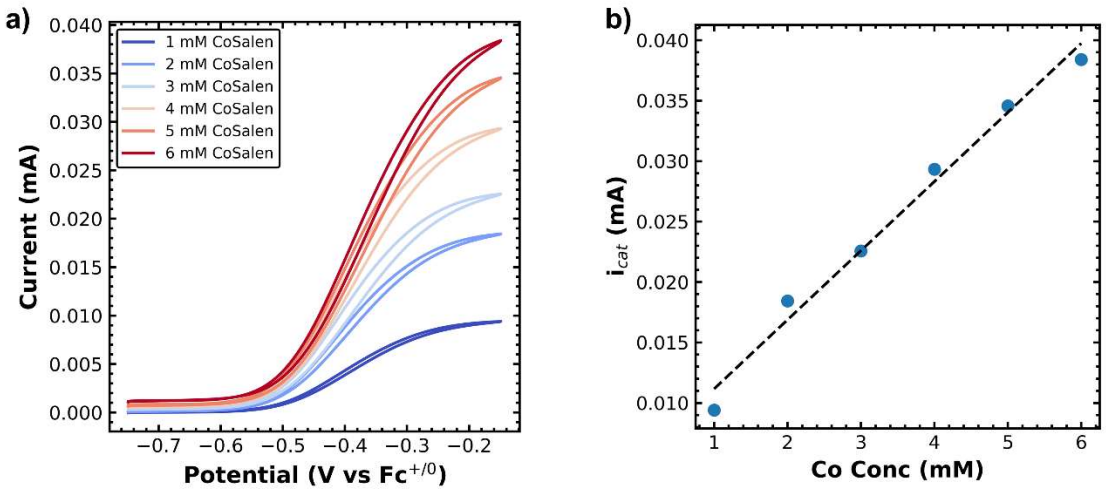

Figure 2. *a)* Representative cyclic voltammograms of varying Co(Salen) concentrations with 1000 equiv. of phenylsilane in a solution of 0.1 M $TBAPF_6$ in DMF with a glassy carbon working electrode at 10 mV/s. *b)* Peak current analysis of the varying Co(Salen) concentrations; the linear dependence on concentration indicates the mechanism is first-order in the catalyst.

The overall mechanism at high silane concentration can be summarized as in **Scheme 3,** where the RDS is the hydride transfer step (step 2). Since step 3 is not rate determining, we can treat this reaction as EC' and utilize established equations to approximate the rate constant of hydride formation. Equation 1 can be normalized by the Randles-Sevcik equation (which describes the peak current's dependence on scan rate for the oxidation of Co(Salen) in the absence of phenylsilane) [23]:

$$\frac{i_{cat}}{i_p^0} = \frac{1}{0.446}\left(\frac{RT}{nF\nu}k_1 C_A\right)^{1/2} \quad (2)$$

where i_p^o is the peak current with no substrate, R is the gas constant, T is temperature, and ν is the scan rate. Using this equation and the slope of the linear region in **Figure 1b,** we can calculate k_1 to be 11 M^{-1} s^{-1}. To our knowledge, this is the first measured rate constant for the hydride transfer step of an MHAT reaction (electrochemical or otherwise) and supports the long-held assertion that such steps are rate-limiting.[13]

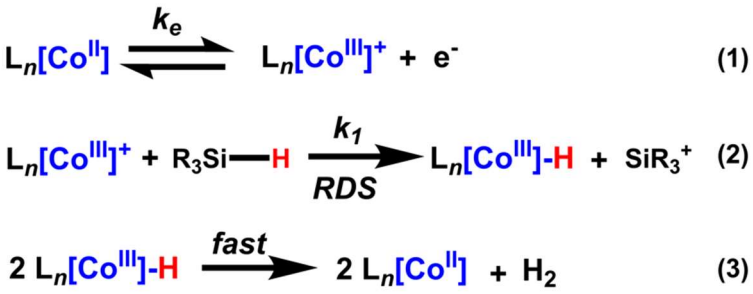

Scheme 3.

We used finite element analysis to simulate the experimental CVs to support these mechanistic assertions and to confirm the accuracy of the measured rate constant. Such simulations provide numerical solutions to Fick's laws of diffusion and homogeneous chemical kinetics and, thus, are ideal for simulating catalytic voltammetry.[23] Using the steps outlined in **Scheme 3**, the experimental CVs were fit best by a simulation with a dimerization rate constant (k_d) of 4 x10^5 M^{-1} s^{-1} and a hydride transfer rate constant (k_1) of 14 M^{-1} s^{-1} (**Figure 3**, see supporting information for full set of simulation parameters and details on *iR* compensation). Agreement between experimental and simulated voltammograms was evaluated on the basis of the peak current as a function of the phenylsilane concentration. The formal potentials were fit from the experimental traces in the absence of phenylsilane. The peak or plateau current for all concentrations of phenylsilane was then simultaneously fit by iteratively varying k_1, $K_{eq,1}$ (equilibrium of the hydride transfer step), and k_d until the magnitude of these simulated currents were within ~10% of the experimental currents at each concentration.

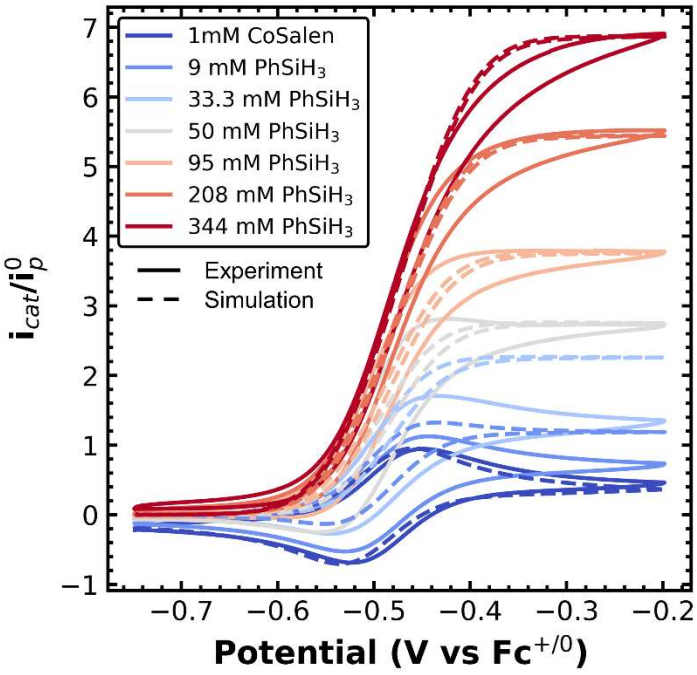

Figure 3. Simulated CVs (dotted lines) at varied phenylsilane concentrations compared to the experimental (solid lines) CVs. Experimental voltammograms taken in a solution of 0.1 M $TBAPF_6$ in DMF with a glassy carbon working electrode at 10 mV/s.

To probe the effects of k_1, $K_{eq,1}$, and k_d on the simulated voltammograms and demonstrate model sensitivity, these values were varied around the best fit values as outlined above. As hydride transfer was predicted to be rate-determining, model sensitivity was first analyzed by computing voltammograms with k_1 varying over the range of 1-50 $M^{-1}s^{-1}$ and k_d = 4x10^5 $M^{-1}s^{-1}$. The simulated peak or plateau (for sigmoidal CVs) current for each concentration of phenylsilane was evaluated and compared to the peaks and plateaus of the experimental voltammogram, shown in **Figure 4a**, revealing high sensitivity to k_1, consistent with hydride transfer as the rate-determining step on the order of k_1 ~ 15 $M^{-1}s^{-1}$. Similar analysis was conducted by varying $K_{eq,1}$ from 1x10^{-4} $M^{-1}s^{-1}$ to 1x10^3 $M^{-1}s^{-1}$ at constant k_1 = 14 $M^{-1}s^{-1}$ and k_d = 4x10^5 $M^{-1}s^{-1}$, (**Figure S5**) and revealed that the current magnitude is sensitive to values of $K_{Eq,1}$ less than 1x10^{-1} $M^{-1}s^{-1}$, above which the model is insensitive to the equilibrium constant. Finally, the model sensitivity to the dimerization process was analyzed by varying k_d between 1x10^3 and 1x10^9 $M^{-1}s^{-1}$. At the best fit k_1 =

14 $M^{-1}s^{-1}$, the currents were relatively insensitive to the value of k_d (**Figure 4b**) above the optimal value of $4x10^5$ $M^{-1}s^{-1}$ but had a significant impact at slower rates, consistent with the expectation that hydride transfer (k_1) is rate limiting. The effects of k_d were also evaluated at k_1 values of 5 and 25 $M^{-1}s^{-1}$, as shown in **Figure S6**. At k_1 = 5 $M^{-1}s^{-1}$, the magnitude of plateau currents at high phenylsilane concentrations was significantly lower than those obtained experimentally, even at k_d approaching the diffusional limit for bimolecular reactions (i.e., ~$1x10^{10}$ $M^{-1}s^{-1}$). At k_1 = 25 $M^{-1}s^{-1}$, while the plateau magnitude for high concentrations could be fit with $k_d < 4x10^5$ $M^{-1}s^{-1}$, the peak behavior at low concentrations of phenylsilane was significantly overestimated. At the best fit of k_1 = 14 $M^{-1}s^{-1}$, the voltammetric behavior could be captured reasonably well with $k_d = 4x10^5$ $M^{-1}s^{-1}$.

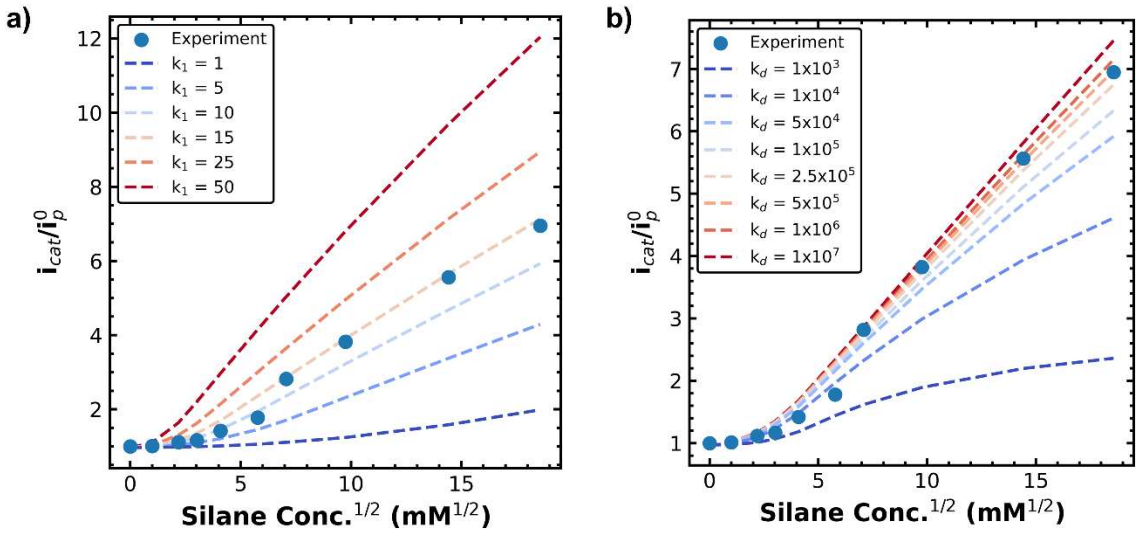

Figure 4. Simulatation of peak currents with *a)* variation of k_1 (hydride transfer rate constant) with k_d at $4x10^5$ $M^{-1}s^{-1}$ and *b)* variation of k_d (dimerization step) with k_1 at 14 $M^{-1}s^{-1}$.

The reasonable agreement of the value of the experimental rate constant and that obtained by simulation, as well as the sensitivity of the model to the magnitude of k_1, and relative insensitivity at high values of k_d, supports the approximation of the mechanism as EC', and thus, the measured rate constant is descriptive of the hydride formation step. It should be noted that simulations had difficulty fitting both

high and low silane concentrations, where there is a clear change in RDS around a phenylsilane concentration of 33 mM (50 eq.) as discussed earlier. The difficulty in fitting both these regions with simulation suggests that that dimerization step is initially slow due to the small Co(III)-H concentration, possibly due to side reactions with trace moisture or impurities. Metal-hydrides are notoriously moisture sensitive, and even trace water can lead to their decay. In fact, early attempts to do these mechanistic studies outside of an inert atmosphere severely limited the catalytic current response.

Controlling rate of Co-H formation with ligand design

Since the voltammetric measurement of k_1 provides a quantifiable metric to describe the rate of hydride formation, we aimed to demonstrate how we can use ligand design to control the rate of Co-H formation. In other words, we want to use this electroanalytical technique to design and quantitatively assess catalyst design. We synthesized a suite of *gem*-dimethyl salen ligands with different functional groups on the *para* position of the phenyl moiety: -OMe, -*tert*-Butyl, -CF_3, -CN, and -NO_2, listed from most electron-donating to most electron withdrawing. The electrocatalytic properties of each complex was then assessed via cyclic voltammetry. First, there was minimal difference in the $E_{1/2}$ of the Co(II/III) couple between the complexes (**Figure S7**), with most within the range of -0.28 to -0.3 V vs $Fc^{+/0}$ (the -NO_2 complex is a slight exception at -0.23 V vs $Fc^{+/0}$). The proximity of these $E_{1/2}$ values indicates these are likely metal-centered oxidations. The more positive value of $E_{1/2}$ for the -NO_2 ligand (highly electron withdrawing) is likely due to the diminished electron density at the cobalt center. Voltammetry of these complexes with increasing amounts of phenylsilane showed that all catalysts exhibited catalytic activity, with a trend correlated to electron donating groups, EDG (-OMe, -*t*Bu) speeding up catalysis and electron withdrawing groups, EWG (-CF_3, -CN, -NO_2) slowing it down (**Figure 5**).

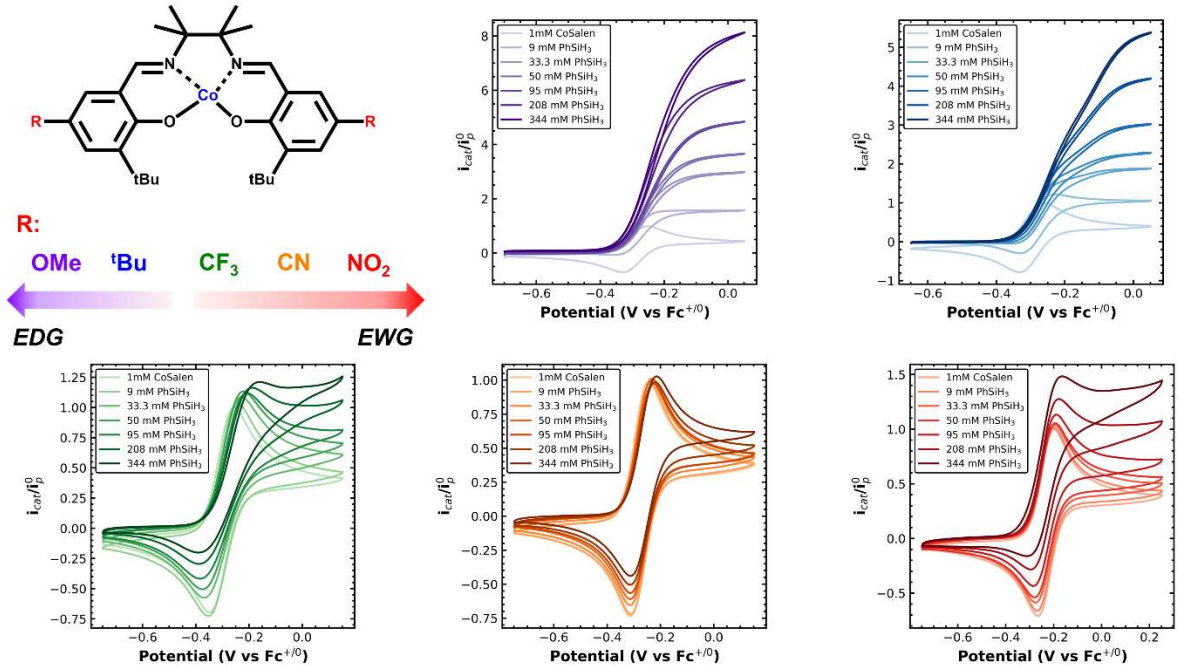

Figure 5. Cyclic voltammograms of functionalized Co(Salen) ligands with increasing amounts of hydride donor phenylsilane. The ligand functional group had a clear impact on the rate of hydride transfer, with electron donating groups increasing the rate of hydride transfer. All voltammograms were taken in a solution of 0.1 M $TBAPF_6$ in DMF with a glassy carbon working electrode at 10 mV/s.

Cyclic voltammetry shows that, generally, the more electron-donating substituents on the catalyst promote catalysis. Peak current analysis with silane concentration (**Figure 6**) displays a characteristic square root concentration at high silane equivalencies for the active catalysts. This indicates the RDS is still the hydride transfer step regardless of the catalyst, and thus changes in the catalytic rate can be taken as changes to the rate of hydride transfer. It is important to note that for the inactive catalysts (e.g., $-CF_3$, -CN), the current plateau after the peak current was used (and not the peak current) to evaluate the rate of hydride formation in the absence of the ideal sigmoidal shape.[23, 31] The plateau current is steady-state, in contrast to the peak current, thus making the plateau current the more accurate descriptor of catalysis. The rate constant for hydride transfer was calculated from the slopes in **Figure 6** using equation

3 for all the catalysts: 11.5 $M^{-1}s^{-1}$ for -OMe, 5.6 $M^{-1}s^{-1}$ for -*t*Bu, 1 $M^{-1}s^{-1}$ for -CF_3, 0.08 $M^{-1}s^{-1}$ for -CN, and 1 $M^{-1}s^{-1}$ for -NO_2.

R group	Measured k_1 ($M^{-1}s^{-1}$)	Simulated k_1 ($M^{-1}s^{-1}$)
OMe	11.5	36
tBu	5.6	13.8
CF_3	1	1
CN	0.08	0.1
NO_2	1	0.96

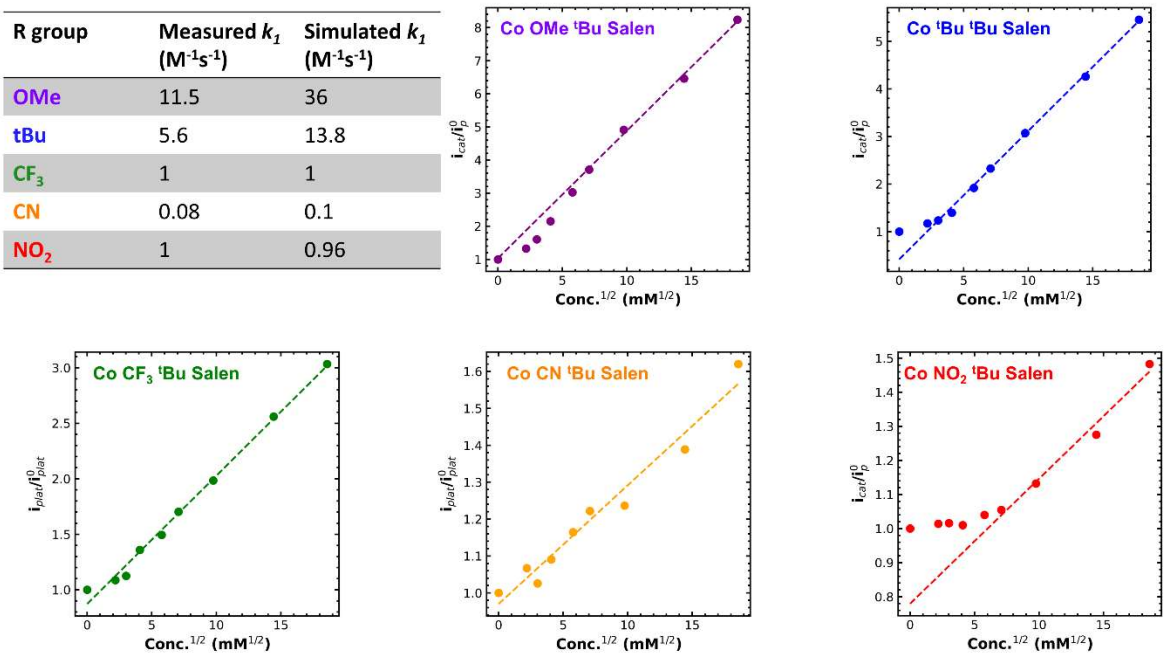

Figure 6. Peak current analysis as a function of phenylsilane concentration for the modified Salen ligands indicating the change in hydride transfer rate, including a comparison of the rate constants measured from experiments and from simulations. Note: for -CF_3 and -CN modified ligands, the post-peak plateau was used to compute the rate constant for hydride transfer.

The voltammetric behavior of each catalyst was simulated and fit to experimental data according to the procedure outlined in the previous section. Simulation of the catalytic CVs (**Figure S8**) showed broad agreement in the slow-down of the hydride transfer step, k_1, with the change in functional group: 36 $M^{-1}s^{-1}$ for -OMe, 13.8 $M^{-1}s^{-1}$ for -*t*Bu, 1 $M^{-1}s^{-1}$ for -CF_3, 0.1 $M^{-1}s^{-1}$ for -CN, and 0.96 $M^{-1}s^{-1}$ for -NO_2. It is interesting to note that the higher the hydride transfer rate constant, the greater the discrepancy between simulated and experimental values. This disagreement arises as hydride transfer rates are increased and the estimation of k_1 using an EC′-type mechanism becomes less accurate as the mechanistic

simplification is less valid. Simulations of the model sensitivity to k_d at a higher value of k_1 (**Figure S6**) support this argument. Still, it is clear that the -OMe functionalized ligand is the fastest for hydride formation, a fact supported in the synthetic literature by increased alkene consumption with the use of -OMe functionalized salen ligands for HAT-based conversions.[6] A possible explanation for the rate increase is the stabilization of the positive charge on the silane generated via hydride transfer to the complex. Mechanistic studies utilizing a variety of silane substrates could help to resolve any substrate-ligand interaction.

The general trend is clearly a decrease in the hydride transfer rate as the ligand substituents are changed from electron-donating to electron-withdrawing. A notable exception is the *increase* in catalytic current moving from the -CN functionalized ligand to -NO_2, possibly due to a change in the RDS from ligand electronics, as suggested by the roughly linear correlation with phenylsilane concentration. Another possibility could be due to the reduction of the -NO_2 group to an EDG, which has been observed for -NO_2 functionalized salen ligand under reductive potentials.[21] Though an electrochemical reduction is not likely at the positive potentials explored here, the silane could act as a reductant to change the ligand electronics (such a reduction would likely impact the $E_{1/2}$ of the complex as silane is added, which is not observed). Another interesting inconsistency in the data is the multiwave shape of the *gem*-dimethyl -*t*Bu voltammogram, which is suggestive of another redox event, possibly an intermediate step in the catalytic cycle and thus highlighting a more complicated mechanism for this catalyst. Regardless, the wide-variability of the hydride transfer step to form the Co-H species suggests a wide range of tunability via ligand electronics for MHAT reactions, an aspect underexplored in the present literature. Other studies using similarly functionalized salen ligands have attributed these changes in reactivity to increases in the rate of recombination of the organic radical and metal catalyst (and the stability of the Co-alkyl bond) during catalysis,[6, 32] and while this is likely to be true, our results indicate that changes to the rate-limiting hydride transfer step also impact selectivity.

Co-H reactivity with alkene substrates

With an understanding of the mechanism of oxidative Co-H *formation* via hydride transfer, we next turned to understanding its *reactivity* with alkene substrates. In the literature, postulated mechanisms for M-H activation can vary substantially, either invoking direct HAT and thereby generating the neutral radical organic species and the original state of the catalyst, or postulating that activation occurs via hydrometallation and the formation of a metal-alkyl intermediate (**Scheme 4**). Other studies recognize that, perhaps, no distinction can be made between these two pathways and an equilibrium exists between the hydrometallation product (M-alkyl intermediate) and the direct HAT product (neutral radical organic species) via reversible homolysis.

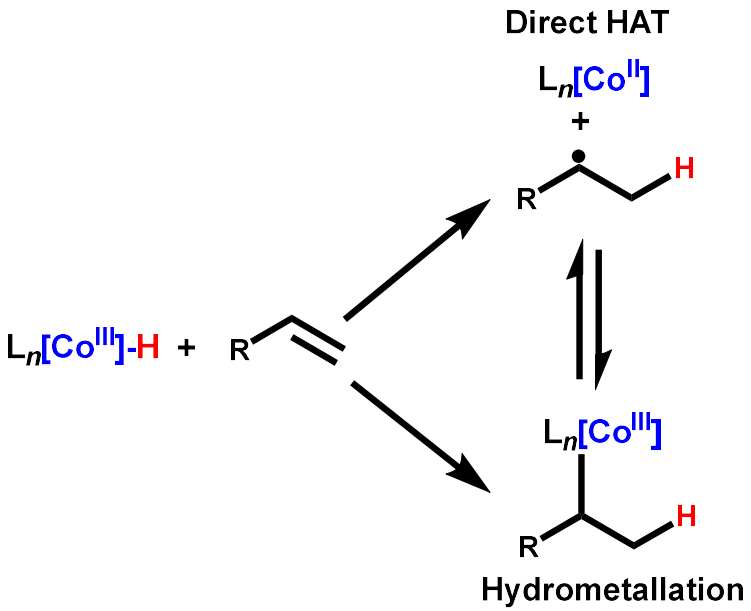

Scheme 4. Possible pathways for alkene activation via Co-H

To this end, we explored the reactivity of the Co-H species via cyclic voltammetry. **Figure 7a** shows the representative CV response of just Co(Salen) (blue), the addition of 110 eq of phenylsilane (light blue), and finally, the addition of 10 eq (light red) and 50 eq (dark red) of 4-tertbutyl-styrene. As discussed above, the addition of phenylsilane promotes the formation of Co-H and its subsequent dimerization resulting a

sigmoidal CV shape, providing a baseline current by which to judge competitive processes due to its enhancement or diminishment. The addition of styrene results in a voltammetric response with diminished current and an anodic shift in $E_{1/2}$; adding additional styrene further diminishes the current and shifts the $E_{1/2}$ anodically.

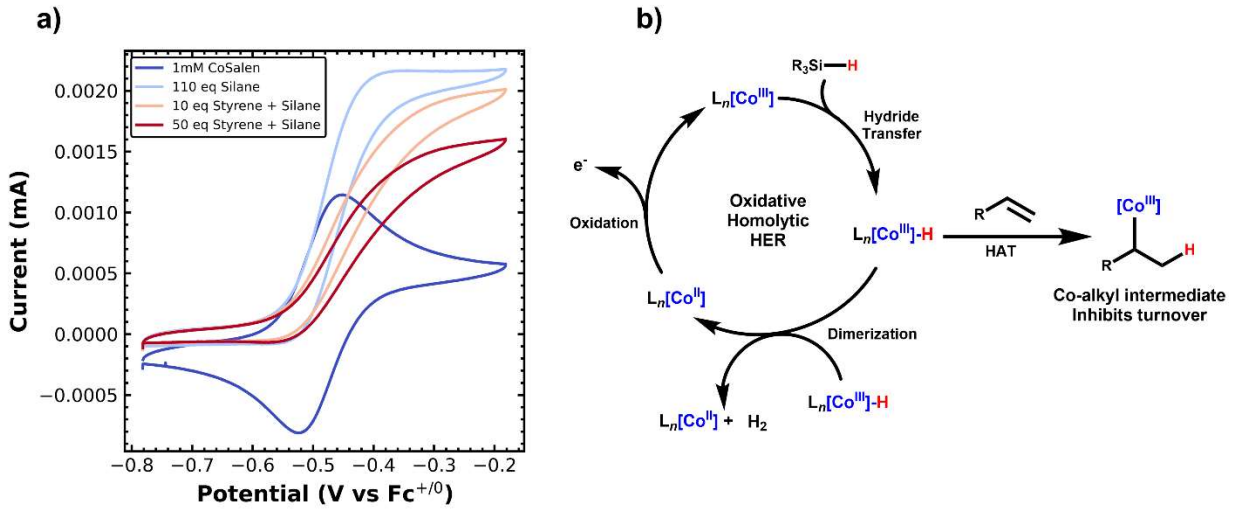

Figure 7. *a)* CVs of CoSalen with phenylsilane and styrene in a solution of 0.1 M $TBAPF_6$ in DMF with a glassy carbon working electrode at 10 mV/s. *b)* Proposed formation of Co-alkyl intermediate.

At first glance, the diminished peak current and anodic shift in potential suggests an ECC mechanism that *does not* return the catalyst to its original state (and disrupts the ECC' HER catalytic cyle). As depicted in **Figure 7b**, this indicates the formation of a Co-alkyl intermediate that inhibits further turnover of Co(Salen) in the oxidative homolytic HER cycle. However, this does not exclude the direct HAT pathway and recombination of Co(II) and the neutral radical. Direct HAT followed by rapid recombination of the metal complex and neutral radical would result in similar voltammetric behavior. In contrast, activation via the direct HAT pathway with no recombination would yield the original form of the catalyst (Co(II)Salen) and thus would exhibit no current decrease or anodic shift (depending on the rate of HAT, which is widely thought in the literature to be a fast step[7, 13]). These results do not favor one

mechanistic pathway over another but simply imply the formation of the metal alkyl intermediate, which inhibits oxidative HER.

As seen above, the current of the homolytic HER cycle provides a way to probe Co-H insertion into the alkene via current decreases and anodic shifts. A solution of Co(Salen) with 0.3 M phenylsilane provided the expected sigmoidal voltammogram after voltammetric cycling (**Figure S9,** Note: cycling resulted in an additional peak neagtive of the catalytic wave, as shown and discussed in **Figure S10a**). We attribute the need for voltammetric cycling to trace moisture or impurities in the system that can react with Co(III)-H and prevent dimerization. Such pre-cycling requirements are common in moisture sensitive systems like redox-flow batteries. After sigmoidal behavior was achieved, the styrene concentration was systematically varied, and the subsequent voltammograms recorded (**Figure 8a**). The resulting plateau current was normalized by the plateau current in the absence of styrene to provide a fractional decrease in current due to Co-H consumption by the alkene. **Figure 8b** illustrates a roughly linear correlation between the normalized peak current decrease and the square root of the alkene concentration, suggesting a first-order process (with respect to alkene concentration). Furthermore, the correlation between the peak current and styrene concentration was independent of the identity of the styrene. Differing substrate identities from EDG (-NMe_2, -MeO) and EWG (-CF_3) on the para-position of the styrene (see **Figure 8** for structures) yielded minimal differences in the measured peak current.

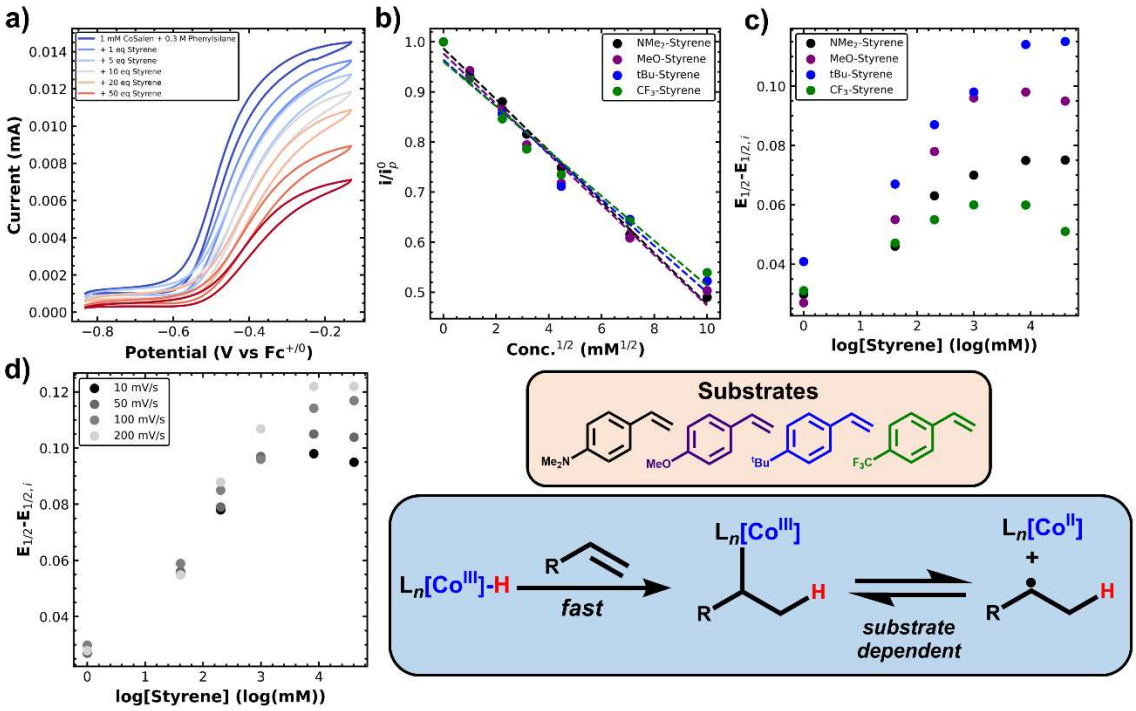

Figure 8. *a)* Representative CVs of CoSalen with phenylsilane and varying amounts of styrene in a solution of 0.1 M $TBAPF_6$ in DMF with a glassy carbon working electrode at 10 mV/s. *b)* Peak current analysis of the different styrene concentrations and different styrene derivatives; peak current diminishment did not depend on styrene identity, indicating hydride formation remains the rate limiting step. *c)* Analysis of the shift in $E_{1/2}$ with increased styrene concentration for different styrene derivatives; the differences in the shift of $E_{1/2}$ for the different derivatives indicate a changing equilibrium between the Co-alkyl intermediate and the neutral radical species. *d)* Representative scan rate dependence of $E_{1/2}$ shift with styrene concentration; the increased $E_{1/2}$ shift at high scan rates and styrene concentration indicates MHAT progresses through a hydrometallation pathway.

Here, the change in peak current can be understood to be a qualitative assessment of the rate of Co-H consumption via the alkene insertion. The rough linear correlation of this change with the square root styrene is the expected result for a first-order molecular process (with respect to styrene). Changing the identity of the styrene with EWG and EDG does *not* impact the rate of Co-H consumption, indicating that the RDS likely remains the hydride formation step via hydride transfer. This observation is consistent with other reports that the hydride transfer step is slow relative to the fast MHAT step and thus rate-

determining for hydrofunctionalization methods.[13] Effectively, the process of forming the metal hydride is the RDS for the whole MHAT process and therefore is the step that must be optimized when considering future ligand and reaction design, a result that underpins the importance of our ability to tune the hydride transfer step via ligand design.

In addition to the current, $E_{1/2}$ is an important descriptor for cyclic voltammetry, as shifts in the half-wave potential can be used to diagnose shifting chemical equilibria during the reaction. **Figure 8c** depicts $E_{1/2}$ subtracted by the initial $E_{1/2}$ before the addition of any styrene ($E_{1/2,i}$) as a function of the log styrene concentration for the same set of different styrene derivatives. Despite minimal differences in the current, there are substantial differences in the $E_{1/2}$ shifts for the different styrene derivatives. **Figure 8d** depicts the representative scan rate dependence of $E_{1/2}$ shifts with styrene concentration. There is minimal difference between scan rates at low styrene concentrations, but at higher styrene concentrations, higher scan rates give larger $E_{1/2}$ shifts, a pattern observed for all styrene derivatives.

The shift in $E_{1/2}$ indicates that the equilibrium is changing as a result of differences in the styrene electronics. To understand these shifts, consider the equilibrium depicted in **Scheme 4** between the Co-alkyl species and the neutral radical: the generation of the neutral radical directly involves the starting state of the catalyst Co(II)Salen, and thus is subject to Nernstian potential shifts based on changes to the Co(II)Salen concentration from equilibria involving Co(II). From the Nernst equation, an increase in the concentration of the reduced species would lead to a cathodic shift in potential and vice versa for the oxidized species. Extending that logic to this system, an equilibrium balance that favors the neutral radical (and thus higher Co(II) concentration) would see *less* positive shifts in $E_{1/2,}$ while a balance that favors the Co-bound species would see *increased* positive shifts in $E_{1/2}$. These shifts are conceptually similar the equilibrium constant-dependent potential shifts studied in CE systems[24]. Thus, the equilibrium constant for this balance can be estimated from these shifts by adapting the equation for CE potential shifts for an oxidation:

$$\ln K_{eq,2} = -\frac{F(E_{1/2} - E_{1/2,i})}{RT} \quad (3)$$

where $K_{eq,2}$ is the equilibrium constant for reversible Co-alkyl bond homolysis (defined such that bond homolysis is the forward step), F is Faraday's constant, R is the gas constant, T is temperature, $E_{1/2}$ is the shifted half-wave potential, and $E_{1/2,i}$ is the half-wave potential before the addition styrene.

The largest shift in $E_{1/2}$ (maximum of ~115 mV, yields $K_{eq,2}$ = 0.01) is found with the *t*Bu-styrene derivative, indicating that it favors (relatively) the bound Co-alkyl intermediate. In contrast, the smallest shift was observed in the CF_3-styrene derivative ($E_{1/2}$ shift of ~60 mV, yields $K_{eq,2}$ = 0.09), indicating that the electron-withdrawing group forces the equilibrium towards the neutral radical species. However, the inclusion of an EDG (-NMe_2 gives $K_{eq,2}$ = 0.05, and -OMe gives $K_{eq,2}$ = 0.02) also appears to shift the equilibrium toward the neutral radical species. Importantly, the general magnitude of the estimated $K_{eq,2}$ are all lower than 1, indicating that the rate of homolysis to the neutral radical species is slower than the backwards rate of recombination, and that all derivatives have an equilibrium that favors the Co-alkyl species, at least for the aryl species explored here. In addition, the resulting trend in EDG to EWG of $K_{eq,2}$ can be characterized as a 'broken' (i.e. non-linear) Hammett correlation. Such non-linearity can be attributed to the stability of the resultant radical species, as both EWG and EDG stabilize organic radicals.[33] However, non-linear Hammett correlations can arise whenever there is a change in RDS,[34] transition state,[35] or resonance stabilization.[36] More in-depth studies using a wide structural array of alkene substrates, different catalysts, Hammett correlation, and machine learning methods[37] are underway and will be crucial in determining the parameters that govern reversible Co-C bond homolysis in electroorganic systems.

These $E_{1/2}$ shifts exhibit a scan rate dependence at high styrene concentrations. At faster scan rates, larger $E_{1/2}$ shifts are observed, while slower scan rates give a smaller shift in $E_{1/2}$. As described above, larger shifts in $E_{1/2}$ can be correlated to an equilibrium favoring the bound Co-alkyl intermediate. The

larger shifts at faster scan rates suggest that at shorter time scales, the equilibrium is shifted towards the bound Co-alkyl intermediate, and at longer time scales (slower scan rates), it is shifted towards the neutral radical species. These results strongly suggest that the MHAT reaction progresses through the hydrometallation pathway (and bound Co-alkyl intermediate) before undergoing homolysis to liberate Co(II) species. One important caveat is that these observations are only for the stabilized aryl radical from MHAT to styrene. Non-aryl and non-activated alkenes with different electronic and steric configurations could adopt distinct mechanisms.

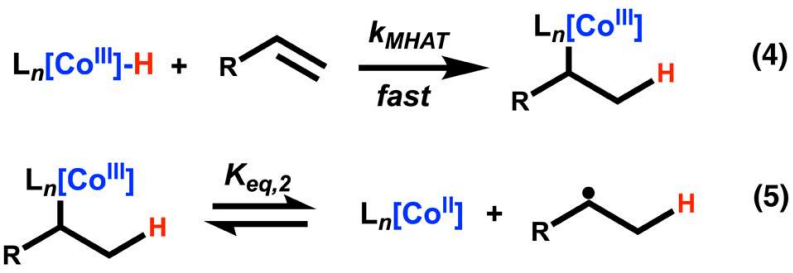

Scheme 5.

With these mechanistic insights in hand, we sought to incorporate the proposed steps into our voltammetric simulations to see if the same trends could be observed. The MHAT and reversible Co-alkyl bond homolysis steps were added to the simulations according to **Scheme 5**, where Co(III)-H insertion into the styrene was treated as fast and irreversible (governed by k_{MHAT}) and Co-alkyl bond homolysis was governed by the equilibrium $K_{eq,2}$ where the forward step is Co-alkyl bond homolysis and the backwards step is radical recombination. The voltammetric behavior observed with the addition of styrene was found to be in agreement with the simulated voltammograms. Incorporation of the MHAT and reversible bond homolysis equilibrium into the kinetic model yielded simulated CVs that were sensitive in current magnitude and $E_{1/2}$ to styrene concentration (**Figure 9a**), similar to the experiments outlined above. In these simulations k_{MHAT} equal to 7×10^2 $M^{-1}s^{-1}$ was found to give the observed current decrease and $E_{1/2}$ shift. Interestingly, this is lower than the rate constant of the competitive dimerization process, k_d.

However, due to the low concentration of Co(III)-H species during catalysis and the relatively higher styrene concentration, this results in a much faster overall rate for MHAT versus dimerization. Next, variation of $K_{eq,2}$ from $1x10^{-3}$ to $1x10^{-6}$ revealed the magnitude of these $E_{1/2}$ shifts were dependent on the magnitude of $K_{eq,2}$ (**Figure 9b**) with smaller values of $K_{eq,2}$ providing larger shifts in $E_{1/2}$, as was observed for the different styrene derivatives. Finally, **Figure 9c** summarizes the dependence of $E_{1/2}$ on styrene concentration for several values of $K_{eq,2}$, which produces a trend similar to that observed for the different styrene derivatives in **Figure 8c.** We emphasize the *qualitative* agreement of our simulations and experiments as a full parametric fit for every styrene derivative at every concentration was not undertaken due to the number of floating parameters at this level of simulation. In particular, the exact magnitude of $K_{eq,2}$ will depend on the balance of k_{MHAT} for the styrene insertion and k_d for dimerization, both of which were estimated via simulation. Nonetheless, the trends observed in these simulations uphold the mechanistic picture derived from our experiments.

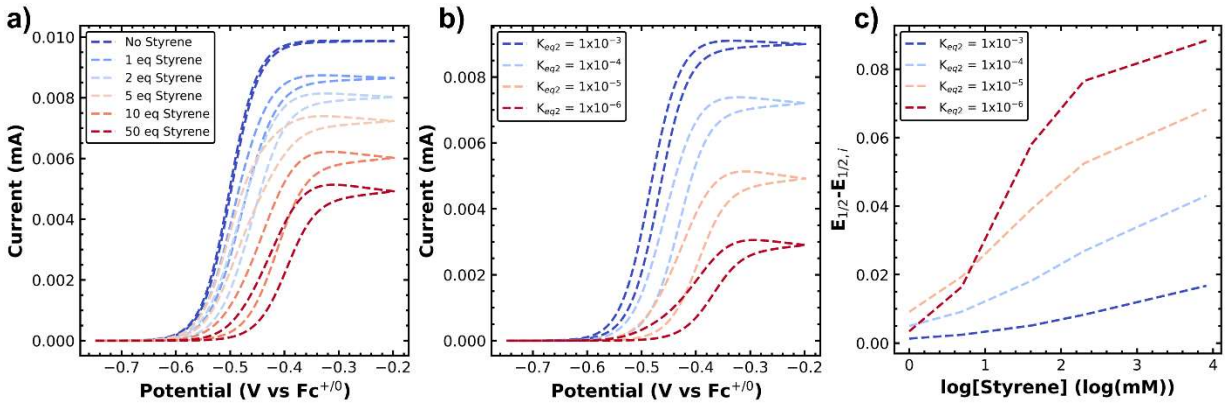

Figure 9. Simulated CVs at varied *a)* styrene concentrations (at $K_{eq,2}$ = $1x10^{-5}$), *b)* varied $K_{eq,2}$ of Co-alkyl bond homolysis at a constant styrene concentration (50 mM), and *c)* the resulting shifts in $E_{1/2}$. Simulations were carried out at 10 mV/s.

Overall, these voltammetric and simulation results show that the bound Co-alkyl intermediate is favored by overall electro-neutral substrates, and the neutral radical is favored (relatively) by the inclusion

of any EWG or EDG, an important point for the design of future reactions. The current decrease and scan rate dependent shifts, regardless of substrate type, suggest that the reaction progresses through the hydrometallation pathway. In all cases, equilibrium constants < 1 were obtained by experiment and simulation, suggesting that the homolysis of the Co-alkyl bond is slow. Likely, this fact is key to the success of MHAT reactions: the formation of the Co-alkyl species can act as a sort of protected radical, where the stable Co-alkyl species prevents decay or homocoupling of the neutral radical species,[38] instead promoting capture by radical electrophiles by keeping the neutral radical concentration low. As noted by others[13] (but not quantitatively investigated), this is effectively a 'persistent radical effect',[39] similar to the strategy employed by nature in coenzyme B_{12}[40]and radical SAM enzymes.[41, 42] Furthermore, the successful integration of secondary catalytic cycles, such as Ni catalyzed C-C coupling[43] or Cu catalyzed cyanation[18], with Co-catalyzed MHAT reactions likely benefit from the initial formation of the Co-alkyl intermediate as transmetallation of the organic substrate from one metal center to the next is proposed as the rate-determining step.[17] More generally, these results demonstrate the power of electroanalytical techniques to study the complex mechanisms of HAT reactions.

3. Conclusions

In summary, we sought to explore the mechanism of Co-catalyzed HAT reactions with electrochemical methods. Using voltammetry and a model homolytic reaction, we observe and measure the oxidative formation of the intermediate Co-H species via hydride transfer from a donor. For the first time, we measured the rate constant of hydride transfer (11 $M^{-1}s^{-1}$) for MHAT and verified this rate with voltammetric simulation. Using a suite of functionalized salen ligands, we demonstrated that the rate of the hydride transfer step is widely tunable via the inclusion of EDG and EWG on the ligand. The reactivity of the Co-H species with aryl alkenes was also explored electrochemically; peak current analysis showed that hydride transfer is the rate-determining step for the full MHAT reaction (at high silane concentrations) and supported the formation of a Co-alkyl intermediate. $E_{1/2}$ shifts were used to

investigate the dynamic equilibrium between the bound Co-alkyl species and the neutral radical organic species; the magnitude of these shifts was highly dependent on the electronic character of the organic substrate, indicating different equilibria between the bound metal-alkyl species and the free radical. In addition, these shifts were scan rate dependent, suggesting that MHAT progresses through the hydrometallation pathway and not direct HAT at least for aryl alkenes. These mechanistic insights highlight the complex reactivity of MHAT intermediates and how reactions can likely utilize one reactive intermediate or the other to give MHAT reactions their distinct diversity. These studies illustrate the power and sensitivity of electrochemical methods for investigating the mechanisms of HAT reactions and provide a strategy for organic chemists to evaluate catalysts and substrate reactivity.

4. Experimental

4.1 Electrochemical Measurements

All electrochemical measurements were conducted under an inert atmosphere in a glovebox with > 0.5 ppm O_2 and moisture content on a Biologic VSP potentiostat. The electrolyte for all experiments was dimethyformamide (DMF, Acros 99.95% Extra Dry) with 0.1 M tetrabutylammonium hexafluorophosphate ($TBAPF_6$, Sigma-Aldrich, >99.0% for electrochemical analysis). Cyclic voltammetry was carried out using a three electrode electrochemical cell with a 0.07 cm^2 glassy carbon working electrode (CH Instruments, CHI 104), a platinum mesh counter electrode (0.5 cm^2, Strem, 99.99%), and a silver wire pseudo-reference electrode (CH Instruments, CHI 112) with a Teflon frit and glass tube filled with electrolyte (0.1 M $TBAPF_6$ in DMF). All measurements were referenced to ferrocene after experiments were finished. Cobalt Salen ((R,R)-(−)-N,N'-Bis(3,5-di-tert-butylsalicylidene)-1,2-cyclohexanediaminocobalt(II), Sigma-Aldrich) was dissolved in 2 mL of electrolyte to achieve a concentration of 1 mM for voltammetric measurements. To this solution was added increasing equivalents of the hydride donor phenylsilane (Sigma-Aldrich, 97%) or triethylsilane (Sigma-Aldrich, 97%) via micro-pipette from a 1 M stock solution also containing 1 mM

Co(Salen) to keep catalyst concentration constant. All concentrations were corrected for dilution. Voltammograms were recorded at 10, 25, 50, 100, 200, and 500 mV/s with the solution mixed thoroughly in between scans to refresh the concentration at the electrode surface. For experiments with the styrene derivatives, an electrolyte solution of 1 mM CoSalen and 0.3 M phenylsilane was prepared (with no gradual titration of phenylsilane). In these experiments without titration of the phenylsilane, the electrolyte solution was cycled voltammetrically in the potential range of interest, -0.8 V to -0.2 V vs $Fc^{+/0}$ 15 times at 10 mV/s until constant sigmoidal voltammetric behavior was observed. For styrene titration, a solution of 0.1 M $TBAPF_6$, 1 mM Co(Salen) (to keep catalyst concentration constant), and 1 M of the styrene derivative (4-*tert*butylstyrene, 4-methoxystyrene, 4-dimethylaminostyrene, 4-trifluorostyrene) was prepared and added to the 2 mL of cycled electrolyte solution in various aliquots via micropipette. Voltammetric scans were recorded at 10, 25, 50, 100, and 200 mV/s for each concentration. Square wave voltammetric experiments utilized a pulse height of 50 mV, a pulse width of 50 ms, and step height of 10 mV with a potential range of -1.4 V to -0.6 V vs $Fc^{0/+}$.

4.3 Comsol Simulations

To probe the kinetics and thermodynamics of oxidatively generated cobalt hydride species, *i-E* traces were simulated using a commercial finite element method (FEM) package, COMSOL Multiphysics 5.5. A time-dependent solver configuration using the Transport of Diluted Species module was employed for all simulations. All simulations were conducted on a computer equipped with an Intel Core i7 930 CPU (2.80 GHz) and 24 GB of RAM. A full summary of simulation parameters is provided in the supporting information.

4.4 Synthesis of *gem*-dimethyl Co(Salen) Derivatives

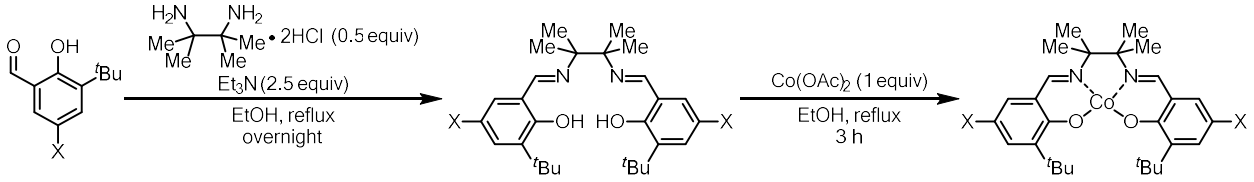

Scheme 5. Synthesis of gem-dimethyl CoSalen Catalysts

Gem-dimethyl Co(Salen) complexes were prepared with the following procedures.

Salen ligand: In a 50 mL round-bottomed flask was charged with diamine hydrochloride salt and aldehyde of interest (X: -OMe, -*t*Bu, -CF_3, -CN, or -NO_2). EtOH (0.1 M vs. aldehyde) was added followed by the addition of triethylamine (2.5 equiv). The mixture was stirred and refluxed for 12h. The resultant mixture was cooled down to room temperature, the solvent was reduced to around 1 mL. A few drops of water were added, and yellow precipitate formed. The precipitate was filtered and washed with cold EtOH/water mixture, then dried at room temperature overnight.

Cobalt complex: Ligand was suspended in EtOH (0.1 M vs. salen) and heated to reflux under nitrogen. After 10 minutes $Co(OAc)_2$ was added and the mixture became red or purple. The reaction mixture was refluxed for 3 hours, cooled to RT and the red precipitate filtered. The purple solid was washed with cold EtOH (10 mL) and dried under high vacuum to afford the cobalt(II) complex.

Acknowledgements

This work was supported by the NSF Center for Synthetic Organic Electrochemistry, CHE-2002158. ADP acknowledges support from the National Science Foundation Graduate Research Fellowship under Grant # 1747505.

Data Availability Statement

All data for additional voltammetric experiments and finite element simulation parameters can be found in the Supporting Information.

References

1. Crossley, S.W., et al., *Mn-, Fe-, and Co-Catalyzed Radical Hydrofunctionalizations of Olefins.* Chem Rev, 2016. **116**(15): p. 8912-9000.
2. Shigehisa, H., et al., *Hydroalkoxylation of unactivated olefins with carbon radicals and carbocation species as key intermediates.* J Am Chem Soc, 2013. **135**(28): p. 10306-9.
3. Gaspar, B. and E.M. Carreira, *Mild cobalt-catalyzed hydrocyanation of olefins with tosyl cyanide.* Angew Chem Int Ed Engl, 2007. **46**(24): p. 4519-22.
4. Lo, J.C., Y. Yabe, and P.S. Baran, *A practical and catalytic reductive olefin coupling.* J Am Chem Soc, 2014. **136**(4): p. 1304-7.
5. Lo, J.C., et al., *Functionalized olefin cross-coupling to construct carbon-carbon bonds.* Nature, 2014. **516**(7531): p. 343-8.
6. Crossley, S.W., F. Barabe, and R.A. Shenvi, *Simple, chemoselective, catalytic olefin isomerization.* J Am Chem Soc, 2014. **136**(48): p. 16788-91.
7. Shevick, S.L., et al., *Catalytic hydrogen atom transfer to alkenes: a roadmap for metal hydrides and radicals.* Chem Sci, 2020. **11**(46): p. 12401-12422.
8. Dadashi-Silab, S. and E.E. Stache, *A Hydrometalation Initiation Mechanism via a Discrete Cobalt-Hydride for a Rapid and Controlled Radical Polymerization.* J Am Chem Soc, 2022.
9. Tilset, M. and V.D. Parker, *Solution Homolytic Bond-Dissociation Energies of Organotransition-Metal Hydrides.* Journal of the American Chemical Society, 1989. **111**(17): p. 6711-6717.
10. Wiedner, E.S., et al., *Thermodynamic Hydricity of Transition Metal Hydrides.* Chem Rev, 2016. **116**(15): p. 8655-92.
11. Jeletic, M.S., et al., *A cobalt-based catalyst for the hydrogenation of CO2 under ambient conditions.* J Am Chem Soc, 2013. **135**(31): p. 11533-6.
12. Smith, D.M., M.E. Pulling, and J.R. Norton, *Tin-free and catalytic radical cyclizations.* J Am Chem Soc, 2007. **129**(4): p. 770-1.
13. Kim, D., et al., *Roles of Iron Complexes in Catalytic Radical Alkene Cross-Coupling: A Computational and Mechanistic Study.* J Am Chem Soc, 2019. **141**(18): p. 7473-7485.
14. Isayama, S. and T. Mukaiyama, *A New Method for Preparation of Alcohols from Olefins with Molecular-Oxygen and Phenylsilane by the Use of Bis(Acetylacetonato)Cobalt(Ii).* Chemistry Letters, 1989(6): p. 1071-1074.
15. Tokuyasu, T., et al., *Co(III)-alkyl complex- and Co(III)-alkylperoxo complex-catalyzed triethylsilylperoxidation of alkenes with molecular oxygen and triethylsilane.* Org Lett, 2002. **4**(21): p. 3595-8.
16. Halpern, J., *Determination and Significance of Transition-Metal Alkyl Bond-Dissociation Energies.* Accounts of Chemical Research, 1982. **15**(8): p. 238-244.
17. Shevick, S.L., C. Obradors, and R.A. Shenvi, *Mechanistic Interrogation of Co/Ni-Dual Catalyzed Hydroarylation.* J Am Chem Soc, 2018. **140**(38): p. 12056-12068.
18. Song, L., et al., *Dual electrocatalysis enables enantioselective hydrocyanation of conjugated alkenes.* Nat Chem, 2020. **12**(8): p. 747-754.

19. Yang, F., et al., *Electrocatalytic Oxidative Hydrofunctionalization Reactions of Alkenes via Co(II/III/IV) Cycle.* Acs Catalysis, 2022. **12**(4): p. 2132-2137.
20. Gnaim, S., et al., *Cobalt-electrocatalytic HAT for functionalization of unsaturated C-C bonds.* Nature, 2022. **605**(7911): p. 687-695.
21. Wu, X., et al., *Intercepting Hydrogen Evolution with Hydrogen-Atom Transfer: Electron-Initiated Hydrofunctionalization of Alkenes.* J Am Chem Soc, 2022.
22. Yan, M., Y. Kawamata, and P.S. Baran, *Synthetic Organic Electrochemical Methods Since 2000: On the Verge of a Renaissance.* Chem Rev, 2017. **117**(21): p. 13230-13319.
23. Bard, A.J., L.F. Faulkner, and H. White, S., *Electrochemical Methods: Fundamentals and Applications, 3rd Edition*. 3 ed. 2022: Wiley. 1104.
24. Savéant, J.M. and C. Costentin, *Elements of Molecular and Biomolecular Electrochemistry*. 2 ed. 2019: John Wiley & Sons Inc.
25. Elgrishi, N., D.A. Kurtz, and J.L. Dempsey, *Reaction Parameters Influencing Cobalt Hydride Formation Kinetics: Implications for Benchmarking H(2)-Evolution Catalysts.* J Am Chem Soc, 2017. **139**(1): p. 239-244.
26. Kurtz, D.A., et al., *Redox-Induced Structural Reorganization Dictates Kinetics of Cobalt(III) Hydride Formation via Proton-Coupled Electron Transfer.* J Am Chem Soc, 2021. **143**(9): p. 3393-3406.
27. Rountree, E.S., et al., *Evaluation of homogeneous electrocatalysts by cyclic voltammetry.* Inorg Chem, 2014. **53**(19): p. 9983-10002.
28. Chalkley, M.J., P. Garrido-Barros, and J.C. Peters, *A molecular mediator for reductive concerted proton-electron transfers via electrocatalysis.* Science, 2020. **369**(6505): p. 850-854.
29. Derosa, J., P. Garrido-Barros, and J.C. Peters, *Electrocatalytic Reduction of C-C pi-Bonds via a Cobaltocene-Derived Concerted Proton-Electron Transfer Mediator: Fumarate Hydrogenation as a Model Study.* J Am Chem Soc, 2021. **143**(25): p. 9303-9307.
30. Costentin, C. and J.-M. Savéant, *Multielectron, Multistep Molecular Catalysis of Electrochemical Reactions: Benchmarking of Homogeneous Catalysts.* ChemElectroChem, 2014. **1**(7): p. 1226-1236.
31. Saveant, J.M. and E. Vianello, *Potential-sweep chronoamperometry: Kinetic currents for first-order chemical reaction parallel to electron-transfer process (catalytic currents).* Electrochimica Acta, 1965. **10**(9): p. 905-920.
32. Chiang, L., et al., *Tuning ligand electronics and peripheral substitution on cobalt salen complexes: structure and polymerisation activity.* Dalton Trans, 2014. **43**(11): p. 4295-304.
33. Nau, W.M., H.M. Harrer, and W. Adam, *Radical Stabilization and Ground State Polar Substituent Effects in the Thermal Decomposition of Azoalkanes.* Journal of the American Chemical Society, 1994. **116**(24): p. 10972-10982.
34. Brennan, M.R., D. Kim, and A.R. Fout, *A synthetic and mechanistic investigation into the cobalt(i) catalyzed amination of aryl halides.* Chem. Sci., 2014. **5**(12): p. 4831-4839.
35. Young, P.R. and W.P. Jencks, *Separation of Polar and Resonance Substituent Effects in the Reactions of Acetophenones with Bisulfite and of Benzyl Halides with Nucleophiles.* Journal of the American Chemical Society, 1979. **101**(12): p. 3288-3294.
36. Um, I.H., et al., *Nonlinear Hammett plots in pyridinolysis of 2,4-dinitrophenyl X-substituted benzoates: change in RDS versus resonance contribution.* Org Biomol Chem, 2010. **8**(16): p. 3801-6.
37. Sandford, C., et al., *Mechanistic Studies into the Oxidative Addition of Co(I) Complexes: Combining Electroanalytical Techniques with Parameterization.* J Am Chem Soc, 2019. **141**(47): p. 18877-18889.
38. Fischer, H., *Unusual Selectivities of Radical Reactions by Internal Suppression of Fast Modes.* Journal of the American Chemical Society, 1986. **108**(14): p. 3925-3927.

39. Fischer, H., *The persistent radical effect: a principle for selective radical reactions and living radical polymerizations.* Chem Rev, 2001. **101**(12): p. 3581-610.
40. Halpern, J., *Mechanisms of coenzyme B12-dependent rearrangements.* Science, 1985. **227**(4689): p. 869-75.
41. Broderick, J.B., et al., *Radical S-adenosylmethionine enzymes.* Chem Rev, 2014. **114**(8): p. 4229-317.
42. Brown, A.C. and D.L.M. Suess, *Reversible Formation of Alkyl Radicals at [Fe4S4] Clusters and Its Implications for Selectivity in Radical SAM Enzymes.* J Am Chem Soc, 2020. **142**(33): p. 14240-14248.
43. Green, S.A., et al., *Branch-Selective Hydroarylation: Iodoarene-Olefin Cross-Coupling.* J Am Chem Soc, 2016. **138**(39): p. 12779-12782.